

See discussions, stats, and author profiles for this publication at: <https://www.researchgate.net/publication/44190356>

# High-Performance TiO<sub>2</sub> Photoanode with an Efficient Electron Transport Network for Dye-Sensitized Solar Cells

ARTICLE *in* THE JOURNAL OF PHYSICAL CHEMISTRY C · SEPTEMBER 2009

Impact Factor: 4.77 · DOI: 10.1021/jp9041974 · Source: OAI

---

CITATIONS

71

READS

121

## 6 AUTHORS, INCLUDING:



Shanqing Zhang

Griffith University

122 PUBLICATIONS 2,828 CITATIONS

[SEE PROFILE](#)



Huijun Zhao

Griffith University

308 PUBLICATIONS 6,323 CITATIONS

[SEE PROFILE](#)



Porun Liu

Griffith University

84 PUBLICATIONS 1,178 CITATIONS

[SEE PROFILE](#)

# High-Performance TiO<sub>2</sub> Photoanode with an Efficient Electron Transport Network for Dye-Sensitized Solar Cells

Hua Yu,<sup>†</sup> Shanqing Zhang,<sup>\*,†</sup> Huijun Zhao,<sup>†</sup> Bofei Xue,<sup>†</sup> Porun Liu,<sup>†</sup> and Geoffrey Will<sup>‡</sup>

*Australian Rivers Institute and The Griffith School of Environment, Gold Coast Campus, Griffith University, QLD 4222, Australia, and School of Physical and Chemical Sciences, Queensland University of Technology, GPO Box 2434, Brisbane, QLD 4001, Australia*

Received: May 5, 2009; Revised Manuscript Received: July 28, 2009

A titanium organic sol was synthesized for the modification of conventional porous TiO<sub>2</sub> photoanodes for dye-sensitized solar cells (DSSCs). As a result, a compact thin TiO<sub>2</sub> film was superimposed on the porous TiO<sub>2</sub> structure as an efficient electron transport network, covering bare conducting substrate surface (FTO) and bridging gaps between TiO<sub>2</sub> nanoparticles, which was confirmed by scanning electron microscope (SEM) and transmission electron microscope (TEM). Dark current measurement suggested that the sol modified photoanode had a remarkably slower recombination rate of the photoelectrons due to the reduced bare FTO surface in comparison with the porous photoanode. The network facilitates the electron transfer in the DSSC process by removing the dead ends of electron pathways, connecting gaps along the electron pathways, and physically enlarging electron pathways, which can be demonstrated by the performance improvement of photocurrent and open-circuit potential. Consequently, the overall energy conversion efficiency of the DSSC was significantly enhanced by 28% after this simple and low-cost organic sol modification. The significant performance improvements observed from the organic sol modified DSSCs suggest that the proposed modification method is a promising alternative to the traditional TiCl<sub>4</sub> modification method.

## 1. Introduction

TiO<sub>2</sub> photoanode plays an important role on determining the performance of a dye-sensitized solar cell (DSSC).<sup>1–3</sup> A typical photoanode for DSSC applications commonly consists of a porous TiO<sub>2</sub> layer coated on conducting substrate (i.e., FTO) with adsorbed dye (e.g., N719) at the TiO<sub>2</sub> surface.<sup>1</sup> The porous TiO<sub>2</sub> layer essentially serves the purposes of collecting and transporting photoelectrons injected by the photoexcited dye via TiO<sub>2</sub> conduction band to the conducting substrate then to the external circuit. High porosity and suitable pore sizes of the porous TiO<sub>2</sub> layer enhance the dye adsorption capacity and light-scattering ability, which imparts high light-harvesting yield and energy conversion efficiency.<sup>4</sup> Nevertheless, a photoanode constructed with the nanoporous TiO<sub>2</sub> layer has several drawbacks. The porous nature of the TiO<sub>2</sub> layer could leave a portion of FTO conducting surface uncovered (see Figure 1a).<sup>5</sup> This allows the redox electrolyte solution to penetrate the porous structure to reach the uncovered FTO surface.<sup>6</sup> The exposure of the conducting FTO surface to the redox electrolyte permits the direct electrochemical reduction of I<sub>3</sub><sup>–</sup> at the interface, leading to the consumption of the photogenerated electron, so-called “electron leakage”.<sup>7</sup> This process, in effect, is equivalent to the direct recombination of photoelectron with excited dye, resulting in dramatically reduced energy conversion efficiency.<sup>8</sup> To date, extensive investigations have been conducted to minimize the electron leakage.<sup>7,9</sup> In this regard, the blocking layer strategy has demonstrated a significant positive effect in reducing the electron leakage.<sup>10</sup> Another drawback of the porous TiO<sub>2</sub> layer is the insufficient connectivity between TiO<sub>2</sub>

particles.<sup>11,12</sup> The connectivity among particles drops significantly within a highly porous TiO<sub>2</sub> layer.<sup>12,13</sup> The decrease in the connectivity or the increase in electron transfer resistance intensifies the photoelectron recombination hence reduces energy conversion efficiency.<sup>12</sup> As illustrated in Figure 1a, the photoelectrons transport across the nanoporous TiO<sub>2</sub> layer via the TiO<sub>2</sub> network (i.e., electron pathways) formed by the interconnected TiO<sub>2</sub> particles and conducting substrate. However, some of these particles may not be interconnected, which results in a limited number of effective electron pathways that have the shortest distance and lowest resistance.<sup>11–13</sup> A longer electron pathway obviously has a higher resistance and larger probability of recombination.<sup>13</sup> Furthermore, there may also be the case in which some TiO<sub>2</sub> particles are even isolated from any electron pathway that is connected to the conducting substrates (i.e., particles marked with “Iso” in Figure 1a). The photoelectrons injected to these dead-ended locations could only be consumed via the recombination process with surface adsorbed dyes in their excited states and/or through a direct electrochemical reaction with I<sub>3</sub><sup>–</sup> at the TiO<sub>2</sub>/solution interface.<sup>12</sup> It is believed that the loss of energy conversion efficiency due to the poor connectivity could be as severe as the loss caused by the electron leakage. However, to this end, the effect of nanoporous structure on the connectivity and energy conversion efficiency has not been sufficiently investigated.<sup>12</sup>

In this article, we propose a simple modification method that can superimpose a compact blocking layer as an efficient electron transport network to a conventional TiO<sub>2</sub>/FTO photoanode fabricated with commercial TiO<sub>2</sub> paste (see Figure 1b). The method employs a titanium organic sol as the coating solution to cement the TiO<sub>2</sub> nanoparticles together and form a thin layer of dense coating at the TiO<sub>2</sub>/FTO interface. We expect such a new structural configuration will be able to collectively tackle the electron leakage and low electron transport efficiency

\* To whom correspondence should be addressed. Phone: +61-7-5552 8261. Fax: +61-7-5552 8067. E-mail: s.zhang@griffith.edu.au.

<sup>†</sup> Griffith University.

<sup>‡</sup> Queensland University of Technology.

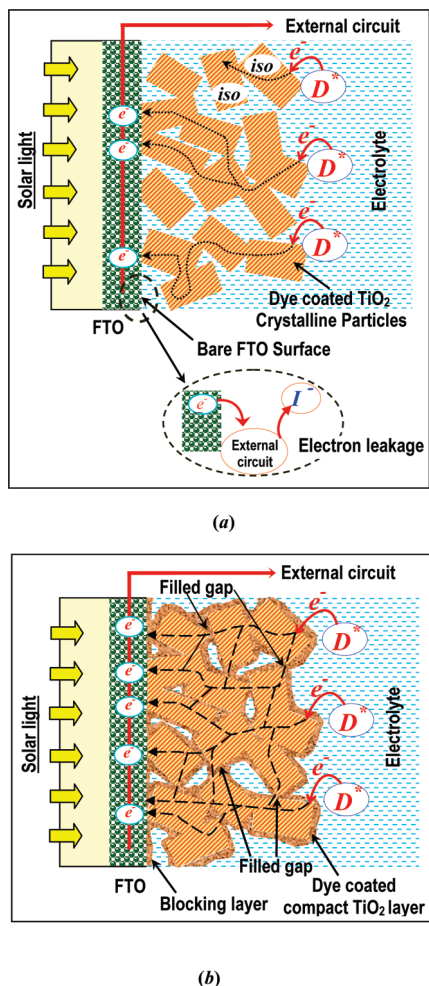


**Figure 1.** Schematic diagrams of electron pathways of the porous structure (a) and sol modified structure (b).

problems experienced by the conventional porous  $\text{TiO}_2$  layers. Improved electron transfer efficiency and hence a higher energy conversion efficiency is expected because of the widened electron pathways and additional electron pathways from the bridging-gap effect that reduce the scattering of free electrons among interparticles.<sup>11,14</sup>  $\text{TiCl}_4$  post-treatment has been a common modification method to improve the performance of nanoporous  $\text{TiO}_2$  films in DSSCs.<sup>15–17</sup> For comparison, the nanoporous  $\text{TiO}_2$  films were also modified by using the  $\text{TiCl}_4$  post-treatment method. The performance of such photoanodes in DSSC was characterized and compared with that of the sol modified photoanodes.

## 2. Experimental Section

**2.1. Materials.** Titanium butoxide, diethanolamine, anhydrous acetonitrile, 1-butanol, and chloroplatinic acid hexahydrate ( $\text{H}_2\text{PtCl}_6 \cdot 6\text{H}_2\text{O}$ ,  $\geq 37.5\%$  as Pt) were purchased from Sigma-Aldrich. Ethanol and 2-propanol were available from Ajax Finechem and Merck, respectively.  $\text{H}_2\text{O}$  was purified by distillation and filtration (Milli-Q).  $\text{TiO}_2$  paste (DSL 18NR-T), N719 dye ( $\text{RuL}_2(\text{NCS})_2 \cdot (\text{H}_2\text{O})_4(\text{TBA})_2$ , 1,2,2'-bipyridyl-4,4'-dicarboxylic acid, TBA-tetrabutylammonium), and liquid electrolyte (EL141) containing  $\text{I}^-/\text{I}_3^-$  redox couple were supplied by Dyesol Co (Australia). Fluorine-doped tin oxide (FTO) glass ( $\leq 14$  ohm/square) was from Pilkington. All materials are analytical grade in this work if not specified.

**2.2. Synthesis of the Titanium Organic Sol.** The titanium organic sol was prepared at room temperature by the method

illustrated in our previous work.<sup>18</sup> Briefly, 68 mL of tetrabutyl titanate and 16.5 mL of diethanolamine were dissolved in 210 mL of absolute ethanol, and then the mixture was stirred vigorously for 1 h at room temperature until a homogeneous solution was formed (solution A). A mixture of 3.6 mL of  $\text{H}_2\text{O}$  and 100 mL of ethanol (solution B) was added dropwise into solution A under rapid stirring. The resulting alkoxide solution, aged for 24 h at room temperature, resulted in an organic sol. The resulting solution was used for the modification of the nanoporous films.

**2.3.  $\text{TiO}_2$  Film Preparation and Modification.**  $\text{TiO}_2$  porous films were screen-printed on precleaned FTO glass substrate.<sup>19</sup> The films were dried in an oven at 85 °C for 10 min and then the deposition process was repeated until an appropriate thickness of 12–15  $\mu\text{m}$  was obtained. Then the films were sintered in a furnace at 450 °C for 30 min. The resulting porous  $\text{TiO}_2$  films were designated as control films.

Modification of the control films by using the organic sol was as follows: first, the control films were immersed into the organic sol for 1 min to ensure that the organic sol fully covers the surface of the nanoporous particles and thoroughly infuse into the nanoporous structure. The sol modified films after removal from the sol were dried in an oven at 60 °C in air atmosphere for 10 min and finally sintered at 450 °C for 2 h in a furnace. The resulting  $\text{TiO}_2$  films were designated as sol modified films. The crystalline phase of the sol modified film was found to be pure anatase.<sup>18</sup>

Post-treatment with  $\text{TiCl}_4$  was carried out according to procedures in the literature.<sup>20</sup> Briefly, a 0.05 M  $\text{TiCl}_4$  aqueous solution was prepared in 2 M HCl solution. Freshly sintered  $\text{TiO}_2$  control films were immersed into this solution and stored in an oven at 70 °C for 30 min in a closed vessel. After flushing with distilled water and drying, the electrodes were sintered at 450 °C in an oven for 30 min. The resulting  $\text{TiO}_2$  films were designated as  $\text{TiCl}_4$  modified films.

**2.4. Physical Characterizations.** A scanning electron microscope (SEM, JEOL 890) and a transmission electron microscope (TEM, JEOL 4010) were employed to investigate the morphologies and crystallinity of the control film and modified films.

**2.5. Dye Adsorption and Dye Loading Measurement.** The control and modified films were put into the dye solution ( $3 \times 10^{-4}$  M in butanol and acetonitrile, 1:1, v/v) for 24 h. The dyed films were washed with anhydrous acetonitrile after the adsorption process and then dried in  $\text{N}_2$  flow before measurements. Dye loading measurements were conducted by desorbing the dye molecules from the dye-anchored films in NaOH ethanolic solution ( $10^{-4}$  M).<sup>21</sup> The loading amount was calculated from the absorbance of the completely desorbed dye solutions by the spectrophotometer (Varian, Cary 4500).

**2.6. Solar Cell Assembly and Characterizations.** A series of DSSCs were prepared with traditional sandwich type configuration by using a dye-anchored  $\text{TiO}_2$  film and a platinum counter electrode deposited on FTO glass.<sup>18</sup> A mask with a window area of 0.15  $\text{cm}^2$  was applied on the  $\text{TiO}_2$  film side to define the active area of the cells. A 500W Xe lamp (Trusttech Co, Beijing) with an AM 1.5G filter (Scientech, Canada) was used as the light source. The light intensity was measured by a radiant power meter (Newport, 70260) coupled with a broadband probe (Newport, 70268). The photovoltaic measurements of DSSC were recorded by a scanning potentiostat (Model 362, Princeton Applied Research, US).

The solar energy-to-electricity conversion efficiency ( $\eta$ ) of DSSC is defined by the following equation:<sup>10</sup>

$$\eta = \frac{J_{sc} V_{oc} \text{FF}}{P_{in}} \times 100\% \quad (1)$$

where  $J_{sc}$  is the short-circuit current density under irradiation,  $V_{oc}$  is the open-circuit voltage, FF is the fill factor, and  $P_{in}$  is the input power.

The open-circuit voltage decay (OCVD) technique<sup>22,23</sup> employed for investigating the electron lifetime ( $\tau_n$ ) is conducted by turning off the illumination on DSSC in a steady state and monitoring the subsequent decay of  $V_{oc}$ . The  $\tau_n$  can be obtained by the reciprocal of the derivative of the decay curves normalized by the thermal voltage:<sup>22</sup>

$$\tau_n = -\frac{k_B T}{e} \left( \frac{dV_{oc}}{dt} \right)^{-1} \quad (2)$$

where  $k_B$  is the Boltzmann constant,  $T$  is the absolute temperature,  $e$  is the positive elementary charge, and  $dV_{oc}/dt$  is the derivative of the transient open-circuit voltage.

### 3. Results and Discussion

**3.1. Morphological, Structural, and Phase Compositional Characteristics.** The property of the organic sol is crucial in obtaining the dense blocking layer and a more efficient electron transport network. The organic sol used in this work possesses low surface tension, low viscosity, and high mobility due to the large ethanol content. This allows the organic sol to readily penetrate the entire porous  $\text{TiO}_2$  structure and reach the uncovered FTO surface. The characteristics of low viscosity and rapid solvent evaporation enable the formation of a dense and uniform thin film on the uncovered FTO surface and the porous  $\text{TiO}_2$  surface simultaneously. The thin coating layer is therefore not expected to significantly change the porosity (affecting dye adsorption capacity) of the original nanoporous structure. The post thermal treatment converts the thin film into highly crystalline anatase  $\text{TiO}_2$ . During the coating process, it would be expected that more coating solution would be retained at the joints among the  $\text{TiO}_2$  particles and small gaps between the particles. Via the thermal treatment process, the titanium organic sol retained at these locations can be transformed into highly crystalline  $\text{TiO}_2$  that cements the original porous  $\text{TiO}_2$  particles together. As a result, the enhanced electron transport network is constructed by enlarging the contact area and bridging the gaps among the nanoparticles, as well as at the  $\text{TiO}_2/\text{FTO}$  interface.

Figure 2 shows the SEM images of the control film and the sol modified film. Similar morphological characteristics for both films were observed because the control and the sol modified films share the same bulk structures that were prepared by using the same starting materials and procedures. However, the effect of modification is clearly evidenced by the images shown in panels b, d, e, and f of Figure 2. This is contrasted with the  $\text{TiCl}_4$  modified films where morphological changes could not be identified by SEM analysis. Typical SEM images of the unmodified sample (i.e., the control film) prepared with commercial  $\text{TiO}_2$  paste were shown in Figure 2, panels a and c. These images exhibit a typical nanoporous structure of randomly packed particles across the entire coating layer. The surface morphology was found to be rough and porous (see Figure 2a). The uncovered conducting FTO areas can be observed at locations where pores and gaps formed between  $\text{TiO}_2$  particles and the substrate (see Figure 2c). Most  $\text{TiO}_2$  particles were in regular cuboid shapes with particle sizes ranged from 20 to 30

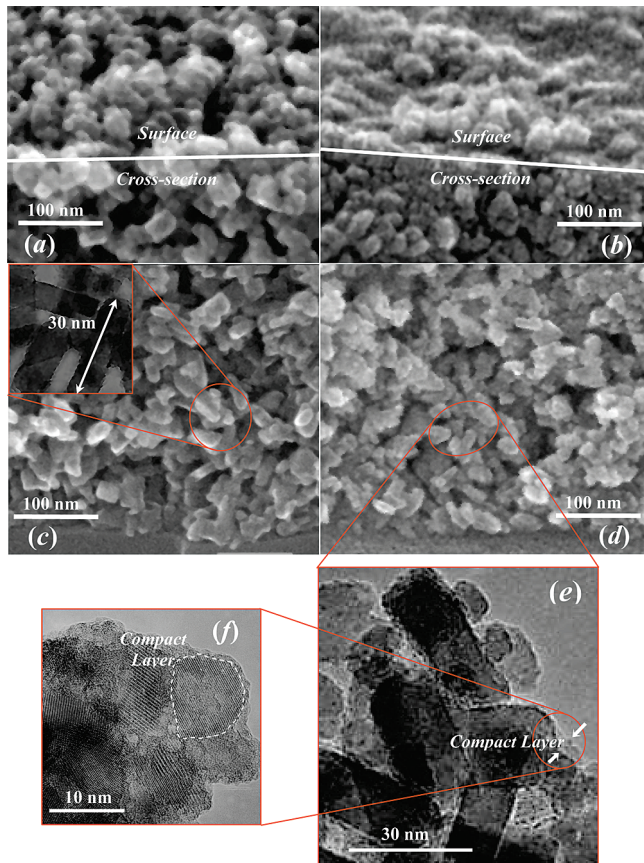


**Figure 2.** SEM and TEM micrographs of control film and sol modified film: (a, b) the cross-sectional micrographs of surface structure for control film and sol modified film, respectively; (c, d) the SEM micrographs of cross-sectional structure for control film and sol modified film, respectively; the inset in part c shows the TEM micrograph of nanoporous structure of control film; (e) the TEM micrograph of sol modified structure; and (f) the TEM micrograph of the compact layer represented in panel e.

nm as shown in the TEM image in the insert of Figure 2c. For a nanoporous structure formed by such randomly packed particles, the important nanoporous structural characteristics such as mean porosity and interparticle connectivity are determined by the size and shape of the original particles.<sup>13</sup> With 20 nm cuboid shaped particles, the mean porosity and interparticle connection number of the random structure were deduced to be 48% and 6, respectively.<sup>13</sup> The SEM and TEM images shown in Figure 2c reveal a large portion of cuboid particles are interconnected via the corner or edge of a particle. The connection areas are deemed to be small due to the sharp corners and edges of the cuboid particles. Because of this, some of the  $\text{TiO}_2$  interparticle networks (i.e., possible electron pathways) may not be fully interconnected with each other and some of them even have dead-ends as they are not connected to the conducting substrates.<sup>12,16</sup> The structure obtained here is very similar to the structure schematically illustrated in Figure 1a.

Panels b and d of Figure 2 show typical SEM images of the modified film prepared by modifying the control sample with the titanium organic sol. These images reveal a nanoporous structure formed with almost identical interparticle frameworks shown in Figure 2a,c. A compact thin coating layer, formed by densely packed small  $\text{TiO}_2$  particles, is visible throughout the entire nanoporous structure, including the surface and the conducting substrate. The overall surface roughness seems similar to those observed from the control film, but the number of large pores at the surface was found to be dramatically

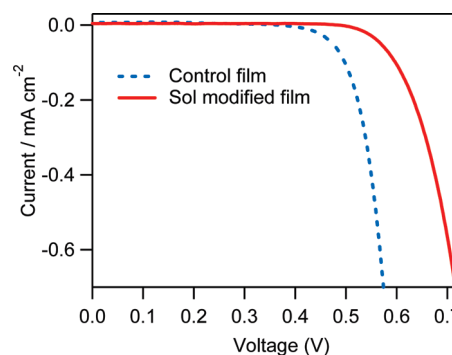
reduced, as a result of the coating layer formation. The improved interparticle connections can be observed from the cross-section image. It can also be seen that the sharpness of the corners and edges of the original cuboid particles were dramatically reduced by the deposited compact layer, suggesting an increase in the interparticle contact areas. These effects can be further confirmed by the TEM image shown in Figure 2f. The TEM image also reveals that the coating layer is more compact and less porous. The thickness of the coating layer depends on the geometry of the location. The coating layer on the individual particle surface was found to be uniform with thicknesses of less than 5 nm. For those interparticle contact areas, especially the contacts via a corner or an edge of the cuboid particle, the compact layer can be as thick as 20 nm (see Figure 2e). For locations at the interparticle gaps, the coating layer thickness depends on the size of the gap. The interparticles gaps less than 5 nm can be completely filled by the organic sol. The structural characteristics observed here are the same as those illustrated in Figure 1b. Nevertheless, further investigations are needed to validate whether these physical and structural improvements can subsequently facilitate the improvement of energy conversion efficiency.

**3.2. Light Reflection and Dye Adsorption.** The modification of the porous structure can influence the DSSC performance from two aspects, one is to produce more photoelectrons, and the other is to improve electron transfer efficiency. The former is normally achieved by enhancing light absorption by amplifying light reflection and boosting dye loading, while the latter is realized by reducing the electron transfer resistance.

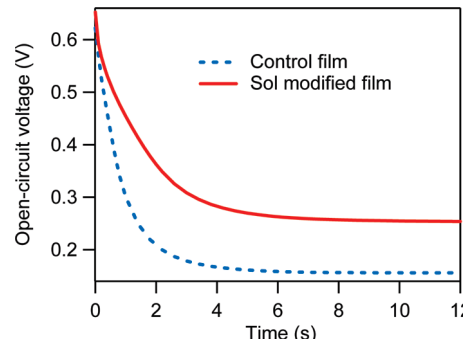
To identify the cause of the performance improvement, the light reflection property and dye loadings of both fabricated electrodes were therefore analyzed. The UV-vis reflection spectra (not shown) indicated that the difference of the reflection properties was very limited. This can be expected because the reflection effect is mainly caused by the large particle sized TiO<sub>2</sub>, e.g., 125 nm,<sup>24</sup> and the size of the sol modified TiO<sub>2</sub> particles in our work was only ca. 10 nm.

Determination of dye loading amount was conducted by desorbing the adsorbed dye from the photoanode into the NaOH ethanolic solution and measuring the absorbance of the solution; the calculated dye loading amounts for the control film and sol modified film were  $1.66 \times 10^{-7}$  and  $1.71 \times 10^{-7}$  mol/cm<sup>2</sup>, respectively. This trivial difference showed that the dye loading was not significantly changed with the modification. The similar dye loading amount implies that under the same illumination condition, the concentration of photoinjected electrons into the TiO<sub>2</sub> conduction band will be the same. Hence, the influence of optical properties of the film and the difference in dye loading after modification cannot justify the changes in the DSSC performance.

**3.3. Electron Leakage.** The electron leakage of DSSC is mainly caused by a back electron transfer process, i.e., the electrochemical reduction of I<sub>3</sub><sup>-</sup> at the exposed FTO surface.<sup>25</sup> Restraining the back electron transfer is vital for enhancing the solar energy conversion efficiency in DSSCs.<sup>15</sup> The electrochemical measurement of dark current can provide valuable information regarding the severity of the back electron transfer process in DSSC. DSSCs with the control film and sol modified film are subjected to the dark current measurement by using a simple linear sweep voltammogram (LSV) test. In this test, potential bias was swept from 0 to 0.75 V and the resulting voltammograms were recorded as presented in Figure 3. The reduction currents originated from the reduction of I<sub>3</sub><sup>-</sup> that penetrated through the film at the bare sites of the FTO surface.<sup>15</sup>



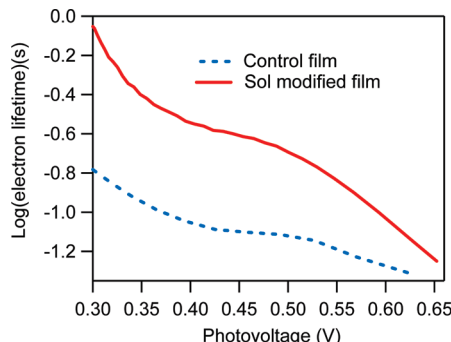
**Figure 3.** Dark currents as a function of applied bias for DSSCs employing the control film and sol modified film.



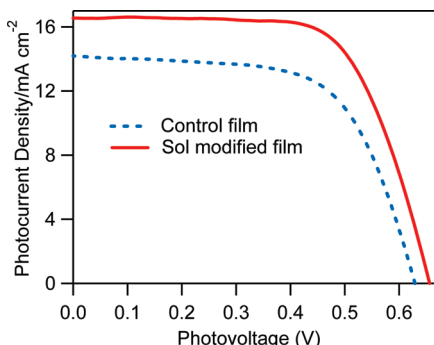
**Figure 4.** Open-circuit voltage decay profiles for DSSCs employing the control film and sol modified film.

Figure 3 shows that the onset of dark current for the control film occurred at ca. 0.45 V, while for the sol modified film, the onset potential shifted to ca. 0.53 V. Furthermore, under the same experimental conditions, for a given potential higher than 0.45 V, the reduction current for the sol modified film drops significantly compared with that of the control film. For example, at a potential of 0.55 V, the dark currents for the sol modified film and the control film were 0.05 and 0.5 mA·cm<sup>-2</sup>, respectively. This means the dark current was reduced by a factor of 10. Because the magnitude of the dark current is directly proportional to the exposed electrode surface area, the increase of the onset potential and the reduction of the dark current demonstrated that the organic sol modification successfully reduced the exposed FTO surface area for the reduction reaction of I<sub>3</sub><sup>-</sup> with the formation of a blocking layer. Therefore, the electron leakage in the DSSC with the sol modified film has been considerably suppressed, which will lead to the better overall photovoltaic performance.

**3.4. Electron Lifetime.** Electron lifetime ( $\tau_n$ ) in DSSC derived from the OCVD measurement<sup>22</sup> has been widely used as a kinetic parameter, which contains useful information on the rate constants of the electron transfer process in DSSC.<sup>23,26</sup> Figure 4 shows the measured OCVD curves of the control film and sol modified film. By applying eq 2, the electron lifetime (in a log representation) as a function of  $V_{oc}$  was plotted in Figure 5. It can be seen that at any  $V_{oc}$ , e.g., 0.6 V, the electron lifetime of the sol modified film was longer than that of the control film, especially in the low open-circuit voltage domain (<0.45 V). The longer electron lifetime of the sol modified film implies a lower charge recombination rate and suggested more efficient electron transfer in the sol modified photoanodes.<sup>23</sup> This improvement of electron transfer efficiency apparently benefits from the optimized electron transfer pathways in the modified structure. The expected electron transfer network shown in Figure 1b has been successfully constructed via the sol modified



**Figure 5.** Electron lifetime (in the log-linear representation) as a function of open-circuit voltage ( $V_{oc}$ ) for DSSCs employing control film and sol modified film.



**Figure 6.** Photocurrents as a function of photovoltage for DSSCs employing the control film and sol modified film.

**TABLE 1: Photovoltaic Characteristics of DSSC Employing Control and Modified Films**

Photoanodes	$J_{sc}$ (mA/cm <sup>2</sup> )	$V_{oc}$ (mV)	FF (%)	$\eta$ (%)
control films	14.18	626	63.9	5.71
sol modified films	16.55	657	67.8	7.32
TiCl <sub>4</sub> modified films	14.91	646	67.9	6.53

film as shown in Figure 2b,d. The improved interparticle connection incorporated with the compact coating layer on the surface and the substrate makes it possible for the photoelectrons in the conduction band to be transferred to the external circuit through the shortest pathway. The shortest pathway for electron transfer, on one hand, reduces the probability for the photoelectrons being recaptured through the recombination, and on the other hand, considerably boosts the transfer velocity of photogenerated electrons in the conduction band to the external circuit. Therefore, the electron lifetime for the sol modified film was significantly extended (see Figure 5) compared with that for the control film.

**3.5. DSSC Performance.** The performance of DSSC with the control film and sol modified film was characterized under the simulated AM 1.5 illumination (100 mW/cm<sup>2</sup>). Photocurrent density as a function of photovoltage ( $J-V$  curves) for DSSC with the control film and sol modified film are shown in Figure 6. The resulting photovoltaic parameters derived from the  $J-V$  curves are listed in Table 1. It shows that, in comparison with the control film, the short-circuit current, open-circuit potential, and fill factor for the sol modified film have been increased by 16.7%, 4.9%, and 6.1%, respectively. This results in an overall 28% increase in energy conversion efficiency.

The short-circuit current density of DSSC is mainly influenced by dye loading amount and electron transfer efficiency in the TiO<sub>2</sub> film.<sup>16</sup> On the basis of the dye loading amount measurement, the difference in dye loading amount between the control

film and sol modified film is negligible. Therefore, the significant increase in short-circuit current density for modified film should be mainly related to the improved electron transfer efficiency in the TiO<sub>2</sub> film. Apparently, this was achieved by the efficient electron transport network shown in Figure 2.

The open-circuit potential of DSSC is directly related to the concentration of electrons in the conduction band. It is mainly limited by recombination of conduction band electrons with I<sub>3</sub><sup>-</sup> ions in the electrolyte and also oxidized dye molecules. The recombination of the conduction band electrons with oxidized dye molecules is negligible in that this process is significantly slower than the regeneration of the sensitizer by I<sup>-</sup>.<sup>27</sup> The suppressed dark current in Figure 3 and the extended electron lifetime in Figure 5 for the sol modified film indicate that the recombination rate of the conduction band electrons is reduced. Therefore, the higher electron concentration in the conduction band and the reduction of recombination rate resulted in the improvement of the open-circuit potential.

### 3.6. Organic Sol Modification vs. the TiCl<sub>4</sub> Modification.

Table 1 shows that, in comparison with the control film, the short-circuit current, open-circuit potential fill factor, and energy conversion efficiency for the TiCl<sub>4</sub> modified film have been increased by 5.1%, 3.2%, 6.2%, and 14.4%, respectively. This suggests that the improvements by the two different post-treatment methods in terms of open circuit potential (i.e., 4.9%) and fill factor (i.e., 6.1%) were comparable. In strong contrast, the improvements in terms of short-circuit current (i.e., 16.7%) and energy conversion efficiency (i.e., 28%) for the sol modified films are substantially higher than that for the TiCl<sub>4</sub> modified films, respectively.

The significantly improved photovoltaic performance for the sol modified DSSC was not likely due to the dye loading difference between the two modification methods. This is because the differences in the amounts of dye loading for the two methods were negligible (see Table S1 in the Supporting Information). More significant performance improvements of the sol modified DSSCs could be due to the following reasons. First, compared with the TiCl<sub>4</sub> solution, the organic sol is able to form more thorough and thicker deposition throughout the film, leading to more effective blocking layer to minimize the electron leakage and constructing more electron pathways. These are evidenced by the fact that the sol modified DSSC had a lower dark current and longer electron lifetime, respectively (see Figures S3–S5 in the Supporting Information). Second, the organic sol modification process is conducted in a relatively mild reaction environment, while TiCl<sub>4</sub> solution is used in a highly acidic solution (i.e., 2 M HCl), which has the potential risk of damaging TiO<sub>2</sub> and FTO surfaces,<sup>28</sup> especially breaking the connection between TiO<sub>2</sub> nanoparticles and the FTO surface.

## 4. Conclusions

An organic sol was employed to modify the structure of nanoporous TiO<sub>2</sub> electrodes. With the modification, an effective electron transport network was constructed. The performance of the DSSC with the sol modified TiO<sub>2</sub> electrode was investigated systematically employing dark-current measurement, photocurrent–voltage ( $J-V$ ) curve, and open-circuit voltage decay (OCVD) technique. It was found that this modification could effectively improve the interfacial connectivity of the nanoporous TiO<sub>2</sub> particles. The resulting increase in the electron transfer efficiency as well as a decrease in the electron leakage through the FTO/electrolyte interface led to an improvement in the energy conversion efficiency in the DSSC. Consequently, the performance of the DSSC with the

sol modified film was significantly improved by 28% compared with that of the control film. The proposed organic sol modification method is a promising alternative to the traditional  $TiCl_4$  modification method.

**Acknowledgment.** The Authors acknowledge the financial support of the ARC discovery grant from the Australian Research Council.

**Supporting Information Available:** Figures showing XRD patterns, absorbance spectra, dark currents as a function of applied bias for DSSCs, open-circuit voltage decay profiles for DSSCs, electron lifetime as a function of opencircuit voltage for DSSCs, photocurrents as a function of photovoltage for DSSCs, and cross-section SEM images and a table giving the dye loading of control film, sol modified film, and  $TiCl_4$  modified film. This material is available free of charge via the Internet at <http://pubs.acs.org>.

## References and Notes

- (1) Gratzel, M. *Nature (London)* **2001**, *414*, 338.
- (2) Nazeeruddin, M. K.; Pechy, P.; Renouard, T.; Zakeeruddin, S. M.; Humphry-Baker, R.; Comte, P.; Liska, P.; Cevey, L.; Costa, E.; Shklover, V.; Spiccia, L.; Deacon, G. B.; Bignozzi, C. A.; Graetzel, M. *J. Am. Chem. Soc.* **2001**, *123*, 1613.
- (3) Hu, L.; Dai, S.; Weng, J.; Xiao, S.; Sui, Y.; Huang, Y.; Chen, S.; Kong, F.; Pan, X.; Liang, L.; Wang, K. *J. Phys. Chem. B* **2007**, *111*, 358.
- (4) Gratzel, M. *J. Photochem. Photobiol., C* **2003**, *4*, 145.
- (5) Zhang, J.; Zaban, A. *Electrochim. Acta* **2008**, *53*, 5670.
- (6) Gregg, B. A.; Pichot, F.; Ferrere, S.; Fields, C. L. *J. Phys. Chem. B* **2001**, *105*, 1422.
- (7) Xia, J.; Masaki, N.; Jiang, K.; Yanagida, S. *J. Phys. Chem. B* **2006**, *110*, 25222.
- (8) Diamant, Y.; Chappel, S.; Chen, S. G.; Melamed, O.; Zaban, A. *Coord. Chem. Rev.* **2004**, *248*, 1271.
- (9) Hart, J. N.; Menzies, D.; Cheng, Y.-B.; Simon, G. P.; Spiccia, L. *C. R. Chim.* **2006**, *9*, 622.
- (10) Peng, B.; Jungmann, G.; Jager, C.; Haarer, D.; Schmidt, H.-W.; Thelakkat, M. *Coord. Chem. Rev.* **2004**, *248*, 1479.
- (11) Mor, G. K.; Varghese, O. K.; Paulose, M.; Shankar, K.; Grimes, C. A. *Sol. Energy Mater. Sol. Cells* **2006**, *90*, 2011.
- (12) Benkstein, K. D.; Kopidakis, N.; Van De Lagemaat, J.; Frank, A. J. *J. Phys. Chem. C* **2003**, *107*, 7759.
- (13) van de Lagemaat, J.; Benkstein, K. D.; Frank, A. J. *J. Phys. Chem. B* **2001**, *105*, 12433.
- (14) Zhu, K.; Neale, N. R.; Miedaner, A.; Frank, A. J. *Nano Lett.* **2007**, *7*, 69.
- (15) Ito, S.; Liska, P.; Comte, P.; Charvet, R.; Pechy, P.; Bach, U.; Schmidt-Mende, L.; Zakeeruddin, S. M.; Kay, A.; Nazeeruddin, M. K.; Graetzel, M. *Chem. Commun. (Cambridge, U. K.)* **2005**, 4351.
- (16) O'Regan, B. C.; Durrant, J. R.; Sommeling, P. M.; Bakker, N. J. *J. Phys. Chem. C* **2007**, *111*, 14001.
- (17) Nazeeruddin, M. K.; Humphry-Baker, R.; Liska, P.; Graetzel, M. *J. Phys. Chem. B* **2003**, *107*, 8981.
- (18) Yu, H.; Zhang, S.; Zhao, H.; Will, G.; Liu, P. *Electrochim. Acta* **2009**, *54*, 1319.
- (19) Tesfamichael, T.; Will, G.; Bell, J.; Prince, K.; Dytlewski, N. *Sol. Energy Mater. Sol. Cells* **2003**, *76*, 25.
- (20) Sommeling, P. M.; O'Regan, B. C.; Haswell, R. R.; Smit, H. J. P.; Bakker, N. J.; Smits, J. J. T.; Kroon, J. M.; van oosmalen, J. A. M. *J. Phys. Chem. B* **2006**, *110*, 19191.
- (21) Liu, X.; Luo, Y.; Li, H.; Fan, Y.; Yu, Z.; Lin, Y.; Chen, L.; Meng, Q. *Chem. Commun. (Cambridge, U. K.)* **2007**, 2847.
- (22) Zaban, A.; Greenshtein, M.; Bisquert, J. *ChemPhysChem* **2003**, *4*, 859.
- (23) Bisquert, J.; Zaban, A.; Greenshtein, M.; Mora-Sero, I. *J. Am. Chem. Soc.* **2004**, *126*, 13550.
- (24) Hore, S.; Vetter, C.; Kern, R.; Smit, H.; Hinsch, A. *Sol. Energy Mater. Sol. Cells* **2006**, *90*, 1176.
- (25) Tennakone, K.; Jayaweera, P. V. V.; Bandaranayake, P. K. M. *J. Photochem. Photobiol., A* **2003**, *158*, 125.
- (26) Bisquert, J.; Vikhrenko, V. S. *J. Phys. Chem. B* **2004**, *108*, 2313.
- (27) Frank, A. J.; Kopidakis, N.; van de Lagemaat, J. *Coord. Chem. Rev.* **2004**, *248*, 1165.
- (28) Ito, S.; Murakami, T. N.; Comte, P.; Liska, P.; Gratzel, C.; Nazeeruddin, M. K.; Gratzel, M. *Thin Solid Films* **2008**, *516*, 4613.

JP9041974